Siderophore coated magnetic iron nanoparticles: Rational designing of water soluble nanobiosensor for visualizing Al^{3+} in live organism

M. Raju, Sakshi Srivastava, Ratish R. Nair, Ishan H. Raval, Soumya Haldar, Pabitra B. Chatterjee

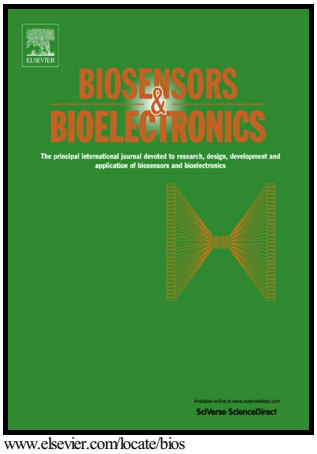

www.elsevier.com/locate/bios

PII: S0956-5663(17)30388-3
DOI: http://dx.doi.org/10.1016/j.bios.2017.06.013
Reference: BIOS9783

To appear in: *Biosensors and Bioelectronic*

Received date: 6 May 2017
Accepted date: 7 June 2017

Cite this article as: M. Raju, Sakshi Srivastava, Ratish R. Nair, Ishan H. Raval Soumya Haldar and Pabitra B. Chatterjee, Siderophore coated magnetic iro nanoparticles: Rational designing of water soluble nanobiosensor for visualizin Al^{3+} in live organism, *Biosensors and Bioelectronic* http://dx.doi.org/10.1016/j.bios.2017.06.013

Siderophore coated magnetic iron nanoparticles: Rational designing of water soluble nanobiosensor for visualizing Al^{3+} in live organism

M. Raju,[†] Sakshi Srivastava,[†] Ratish R. Nair,[†] Ishan H. Raval,[‡] Soumya Haldar,*[‡,§] and Pabitra B. Chatterjee*[†,§]

[†]**Analytical Division and Centralized Instrument Facility, CSIR-CSMCRI, Bhavnagar, Gujarat, India.**

[‡]**Marine Biotechnology and Ecology Division, CSIR-CSMCRI, Bhavnagar, Gujarat, India.**

[§]**Academy of Scientific and Innovative Research, CSIR-CSMCRI, Bhavnagar, Gujarat, India.**

Corresponding author: pbchatterjee@csmcri.res.in

ABSTRACT: This article aims to establish the judicious use of iron-binding chemistry of microbial chelators in order to functionalize the surface of iron nanoparticles to develop non-toxic nanobiosensor. Anchoring a simple siderophore 2,3-dihydroxybenzoylglycine (**H_3L**), which bears catechol and carboxyl functionalities in tandem, on to the surface of Fe_3O_4 nanoparticles has developed a unique nanobiosensor **HL-FeNPs** which showed highly selective and sensitive detection of Al^{3+} in 100 % water at physiological pH. The biosensor **HL-FeNPs**, with 20 nM limit of detection, behaves reversibly and instantly. *In-vivo* bio-imaging in live brine shrimp *Artemia* confirmed that **HL-FeNPs** could be used as fluorescent biomarker for Al^{3+} in live whole organisms. Magnetic nature of the nanosensor enabled **HL-FeNPs** to remove excess Al^{3+} by using external magnet. To our knowledge, the possibility of microbial chelator in the practical development of Al^{3+} selective nanobiosensor is unprecedented.

Graphical abstract

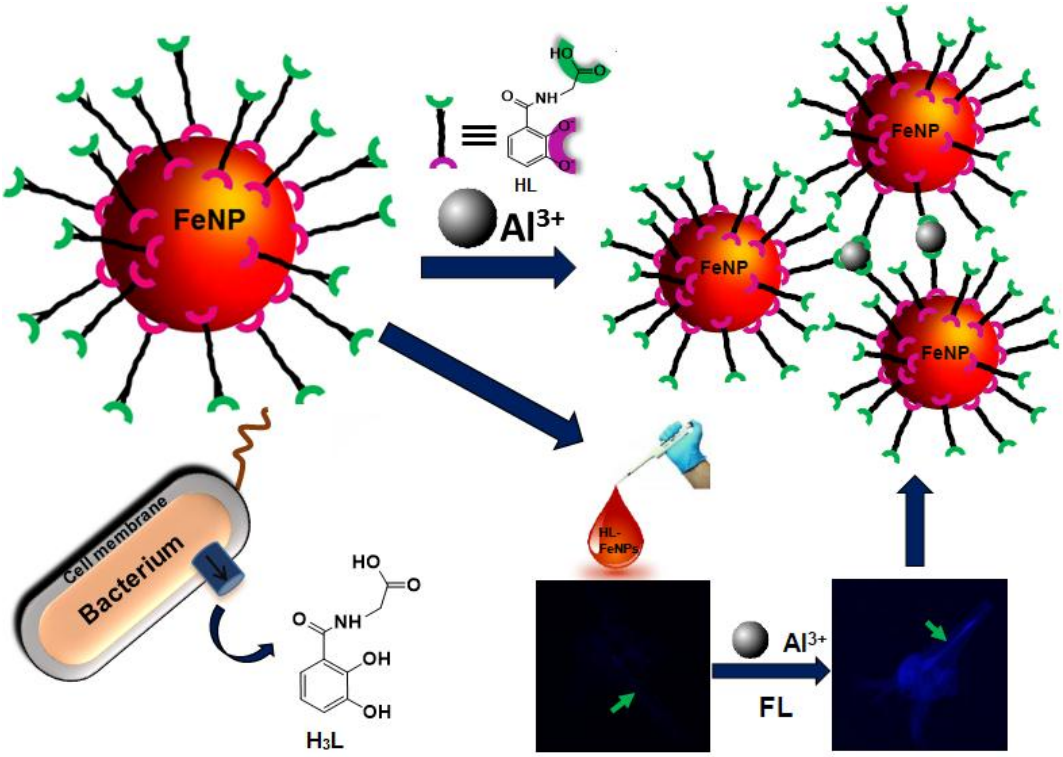

Rational fabrication of iron nanosurface by a siderophore to develop nanobiosensor useful for practical applications and *in-vivo* imaging of Al^{3+} in live whole organism.

Keywords: Siderophore, iron nanoparticles, biosensor for Al^{3+}, removal of Al^{3+}, and live organism imaging.

1. Introduction

Formulations containing components down to nano sizes are important in the applications of nanomaterials for example, use of nanoparticles in biomedical field (Pu et al., 2014; Wang et al., 2012). Nanomaterials, reported in the literature, largely contains Au, Ag, Fe, Cu, Ni, V, Gd, Pd, and Pt-metals and also silica and carbon. Iron nanoparticles (FeNPs), in particular, possess some excellent features viz. superparamagnetic behaviour, great biocompatibility, low-cost, and unique ability to function as contrast agents in magnetic resonance imaging (MRI). After local administrations, FeNPs can be used for targeted drug delivery using external magnets. These key features of FeNPs are often used in imaging (Hu et al., 2016; Wang et al., 2010), thermotherapy (Espinosa et al., 2016), targeted delivery of drugs and DNA (Nel et al., 2009), detection and inhibition of tumour growth (Pal and Alocilj, 2010), gene therapy (Tang et al., 2010), tissue repair (Shubayev et al., 2009), *in-vivo* detection of important biomolecules and their separation (Hasany et al., 2012; Wang et al., 2008). Surface functionalization of bare FeNPs has always resulted remarkable applications of these materials (Wang et al., 2012; Wang et al., 2010; Nel et al., 2009; Wang et al., 2008; Jin et al., 2012; Wang et al., 2011). Surface of bare FeNPs has been exploited to attach foreign molecules as the binding affinities of such molecules vary while anchoring on iron surfaces. In this context, one important class of natural molecule, called siderophores, deserve special attention because of their high binding affinities for iron.

Siderophores are low molecular weight hydrophilic and polar natural molecules (Sandy et al., 2009; Hider and Kong, 2010; Johnstone and Nolan, 2015). The bioavailability of iron in aqueous aerobic environments is limited due to the formation of poorly water soluble polymeric iron hydroxo-aqua complexes which is enough to limit the growth of the microorganisms (Raymond et al., 2003). To manage their physiological needs, microbes synthesize and secrete

microbial chelators which have well-documented role as iron-scavenging materials (Braun and Hantke, 2011; Zheng and Nolan, 2012). Active iron binding motifs, present in siderophores, typically include catecholate, hydroxamate, α-hydroxy carboxylate, and/or carboxylate functional groups. For quite some time, these natural molecules have been receiving great attention in therapeutics (Li et al., 2014; Cochrane et al., 2015; Bugdahn et al., 2010) and bio-imaging applications (Johnstone and Nolan, 2015; Zheng and Nolan, 2014; Zheng et al., 2012; Raju et al., 2015; Raju et al., 2016; Lambert et al., 2000). The siderophore, 2,3-dihydroxybenzoylglycine (**H_3L**, Fig. 1a) is a catechol derived small natural microbial chelator which is produced by the rod-shaped gram-positive bacterium *Bacillus subtilis* NRRL B-1471 when cultured in an iron deficient medium (Ito and Neilands, 1958; Garibaldi and Neilands, 1955). Functionalization of the surfaces of bare FeNPs (Fig. 1b) using **H_3L** has led to the development of a novel nanobiosensor **HL-FeNPs** (Fig. 1c). We observed that the addition of aqueous solution of Al^{3+} to **HL-FeNPs** results a strong emission from the solution mixture.

Aluminium pollution is largely associated with bauxite mining and food-additives/food-packaging borne. Elevated levels of Al^{3+} fluctuates the physiology of cells. This imbalance triggers several human disorders such as dementia, anaemia, and bone diseases. Therefore, considerable efforts have been made in the past 15 years to track Al^{3+} levels by developing the *de novo* design of Al^{3+}-selective receptors. Recently, Das and co-workers have summarized Al^{3+}-selective chemosensors in a review article (Das et al., 2013). However, excluding two chemosensors, all others are purely water insoluble. Thus, posing serious limitations of these probes for practical applications. Since, reports on Al^{3+} specific chemosensors was updated till 2013 in the review article, we have further compiled the literature on Al^{3+} selective optical probes which are completely soluble in 100 % water (Table S1 and S2, see supplementary

materials). As evident from Table S1, small molecule based water soluble probes suffer seriously from interference issue. On the other hand, nanoparticles based probes are aqueous compatible (Table S2) and are not challenged by the interference problem. Obviously, this encouraged us to design and develop Al^{3+} selective biosensor which is derived from nanoparticles. However, with regard to cost, biocompatibility, and removal efficacy FeNPs offer superior choices among different metal nanoparticles, particularly gold and silver. To the best of our knowledge, there is no report in which magnetic FeNPs grafted with a microbial chelator has been developed as an effective Al^{3+} specific biosensor and removal agent as well. To demonstrate the practical use of **HL-FeNPs** as biosensor can work as a staining agent in live organism, we have performed *in-vivo* bio-imaging application of the probe in whole live brine shrimp *Artemia*.

2. Experimental details

*2.1 Synthesis of siderophore functionalized iron nanoparticles **HL-FeNPs***

The catechol functionality bearing microbial chelator i.e. siderophore **H_3L** was synthesized according to the method described in the literature (Soulere et al., 2002). Next, the functionalized iron nanoparticles (**HL-FeNPs**) was synthesized by the following procedure: $Fe(acac)_3$ (0.70 g, 2 mmol) was dissolved in a mixture of benzyl ether (10 mL) and oleylamine (10 mL). The above solution was dehydrated at 110°C for ca. 1 h under a flow of nitrogen and quickly heated to 200 °C for ca. 2 h under a blanket of nitrogen. The resulting black-brown mixture then cooled gradually to room temperature. Next, ethanol (40 mL) was added to the mixture and the precipitates was collected by centrifugation at 8000 rpm and was washed thrice with ethanol. The product was re-dispersed again in hexane. Finally, oleylamine functionalized iron nanoparticles (10 mg) was added to a solution of **H_3L** (50 mg dissolved in 15 mL dichloromethane) and stirred overnight at room temperature. Functionalized iron nanoparticles

(**HL-FeNPs**) was precipitated by centrifugation (8000 rpm, 10 min). Selected IR bands (FTIR-ATR, cm^{-1}) 3100, 1680, 1660, 1594, 1477, 1392, 1300, 1257, 1158, 1074, 929, 889, 748, 684, 630, 595, 505, and 441.

2.2 Brine shrimp Artemia harvesting and bio-imaging studies

Artemia cysts were grown under continuous aeration of sea water. Two different concentrations (5 and 10 μM) of Al^{3+} were prepared in 10 mL HEPES buffer (100 % water, pH 7.4). After 30 minutes hatching of the cysts at 25 °C, the excess Al^{3+} was removed from the culture medium by centrifugation. Following repetitive (couple of times) removal of Al^{3+}, *Artemia* were then exposed to **HL-FeNPs** (concentration: 10 μg iron/mL) taken in HEPES buffer (prepared in 100 % water). In each tube, nearly 30 numbers of *Artemia* were added. After the incubation, *Artemia* was washed with HEPES buffer. Next, individual live *Artemia* was mounted on a glass slide and examined through microscope. For control images, tubes containing **HL-FeNPs** were also used.

3. Results and discussion

*3.1 Synthesis and characterization of **HL-FeNPs***

Catechol based microbial chelator i.e. siderophore **H_3L** was synthesized according to the method previously described in the literature (Soulere et al., 2002) and its characterization details is provided in the supplementary materials (Fig. S1). The formation of Fe_3O_4NPs (called bare iron nanoparticles, FeNPs, Fig. 1b) is reported by the thermal decomposition of $Fe(acac)_3$ in presence of oleylamine (Wang et al., 2008; Xu et al., 2009). Surface functionalization of FeNPs with polar natural molecule **H_3L** was performed by replacing oleylamine and we have used this fabricated nanoparticles i.e. **HL-FeNPs** (Fig. 1c) as such in this work. TEM and FTIR-ATR measurements of **HL-FeNPs** were performed to check whether **H_3L** is successfully anchored on to the surface

of FeNPs. TEM images of the nanoparticles and their size distribution are shown in Fig. 2a and S2. The average size of oleylamine coated bare FeNPs is ~ 4.2 ± 0.6 nm (Fig. S2b). After surface modification of the bare FeNPs with **H_3L**, the average diameter of **HL-FeNPs** changed to ~7.2 ± 1 nm (Fig. S2c).

IR spectra of **HL-FeNPs** (Fig. 2b and Fig. S3) showed pertinent bands at 630, 595, and 441 cm^{-1} due to the Fe-O stretches in Fe_3O_4 moiety (Zhi et al., 2013). The band at 3370 cm^{-1}, due to the O-H stretch of catechol OH groups of free siderophore (**H_3L**), has disappeared upon grafting on the surface of bare FeNPs. This confirms the deprotonation of **H_3L** and its subsequent attachment to the nano-surface. Carboxyl OH stretch at ~3100 cm^{-1} along with a pair of C=O stretches at 1680 and 1660 cm^{-1}, corresponding to the amide C=O and carboxyl C=O groups, respectively, have also been appeared about the same position as observed for free **H_3L**. Thus, indicating the binding of catecholate OO donor sites from **HL^{2-}** on the surface of Fe_3O_4. Moreover, strong band at 1594 cm^{-1}, due to the N-H bending of the siderophore has also appeared in the IR of **HL-FeNPs**. Therefore, further confirms the grafting of the siderophore on the surface of FeNPs.

The hydrodynamic diameters of FeNPs and **HL-FeNPs** were determined by dynamic light scattering (DLS) experiments and were found to be 7 ± 1.5 nm and 9.8 ± 1.8 nm, respectively (Fig. S4 and 2c). DLS measurements were recorded with aqueous samples of the nanoparticles while, TEM experiments were performed with dry nanoparticles. Hence, the observed divergence in diameters was observed by the two techniques. To further investigate the surface functionalization of iron nanoparticles, thermogravimetric analysis (TGA) was performed next. The TGA curves of **H_3L**, FeNPs, and **HL-FeNPs** are shown in Fig. S5. In **H_3L**, 54 % weight loss was observed in the temperature range 100 °C to 400 °C (Fig. S5a). In **HL-**

FeNPs powders, the first weight loss (3 %) until 200 °C was assigned to the adsorbed water (Xian et al., 2013). The second weight loss (48 %) in the range of 200-550 °C was due to the decomposition of the bound siderophore (Fig. S5b). Above 550 °C and up to 900 °C, the oxygen containing portions (13 %) on the nanosurface of Fe_3O_4 was completely removed leaving 36 weight % of magnetite ash (Yang et al., 2017). Comparing Fig. S5a and S5b, the small difference in decomposition temperature (20 °C) indicates adsorption of **H_3L** on the surface of **FeNPs** (Zhou et al., 2017). Therefore, TGA compliments the results from TEM, DLS, and FTIR-ATR. Powder X-ray diffraction (PXRD) experiments with dried bare FeNPs and **HL-FeNPs** exposed sharp diffraction peaks indicating crystalline nature of both (Fig. S6 and 2d). In **HL-FeNPs**, the diffraction peaks at 30.4, 35.77, 43.1, 54, 57.3, and 62.8 ° (2θ) correspond to the [220], [311], [400], [420], [511], and [440] planes of cubic Fe_3O_4 lattice, respectively (Fig. 2d). Similar peaks were also observed in bare FeNPs (Fig. S6) and the results are nicely matching with the standard data of cubic inverse spinel (Sharma et al., 2015). Finally, elemental analysis of **HL-FeNPs** showed C, H, and N stoichiometry as 9:7:1 and therefore, providing conclusive evidence for the presence of deprotonated form of the siderophore on the iron nano-surface.

*3.2 Fluorimetric detection of Al^{3+} by **HL-FeNPs** in 100 % water*

HL-FeNPs is weakly fluorescent in 100 % water but to the naked eye the solution looks to be colourless under visible light. In aqueous medium, **HL-FeNPs** showed three absorption peaks at 222, 246, and 320 nm. Upon excitation of this solution at 340 nm, a weak emission profile was observed. To evaluate the nature of interactions in the excited state of **HL-FeNPs** with different metal ions, emission of **HL-FeNPs** was studied under identical experimental conditions. Most of the metal ions did not show any change in the emission of **HL-FeNPs**. However, on addition of 50 μM Al^{3+} to the aqueous solution of **HL-FeNPs**, a 7-fold

enhancement in the emission peak was observed along with a significant blue shift (33 nm) of the peak (Fig. 3). Sky blue colouration of the aqueous solution of **HL-FeNPs** was also noticed under UV lamp (Fig. S7) with the addition of Al^{3+}. Fig. S8 clearly revealed that enhancement in emission of **HL-FeNPs** occurs on addition of Al^{3+} to it.

Sensory properties of **HL-FeNPs** towards Al^{3+} in the pH range 2-12 was studied next. No apparent changes in the emission spectra of **HL-FeNPs** alone were observed with varying pHs however, **HL-FeNPs** can work well in the pH regime 6-12 (Fig. S9). Therefore, in this study all spectral analyses were performed in HEPES solution (prepared in 100 % water) at pH 7.4. Upon increasing addition of different concentrations of Al^{3+} (0 to 250 μM) to the aqueous solutions of **HL-FeNPs**, the emission intensity of the probe solutions gradually increases (Fig. S10**)**. The fluorescence intensity of the emission peak gets saturated at 200 μM Al^{3+}. Using Benesi-Hildebrand equation (Benesi and Hildebrand, 1949; Wang et al., 2010) and fitting the data points to it, the binding constant (*K*) was determined to be 0.4×10^4 M^{-1} (Fig. S11a). The limit of detection (LOD, Fig. S11b) was found to be 20 nM (0.26 ppb) which is well below the USEPA and the EU standards (~200 ppb) in drinking water (Vallejos et al., 2015).

Selectivity of **HL-FeNPs** towards Al^{3+} in occurrence of other competing metal ions was also explored. Results displayed in Fig. 4, clearly showed fluorescence enhancement of the probe in presence of Al^{3+} and remained unaffected in presence of other metal ions. Therefore, illustrating the unique ability of **HL-FeNPs** as an Al^{3+}-specific nanosensor. Reversible behaviour of **HL-FeNPs** towards Al^{3+} was explored by the introduction of KF to a mixture of **HL-FeNPs** and Al^{3+} (Fig. S12). Moreover, alternate addition of Al^{3+} and KF to the aqueous solution of **HL-FeNPs** showed reusable behaviour of the probe (Fig. S12b). Response time of **HL-FeNPs**

towards Al^{3+} in aqueous solution is quite fast (~ 1 min) as evident from Fig. S13 in which changes of emission peak intensity is plotted as a function of time.

*3.3 Mechanism for the fluorimetric detection of Al^{3+} by **HL-FeNPs***

From TEM imaging, we observed aggregation of the functionalized iron nanoparticles on addition of Al^{3+} (Fig. S14a). As expected, similar observation was also noticed from the DLS experiments. As revealed from Fig. S14b, the hydrodynamic diameter of **HL-FeNPs** is increased to 1060 nm on addition of Al^{3+} (Sharma et al., 2015). Negative zeta potential (ζ) of **HL-FeNPs** (-10.23 mV) changed to a positive value (3.25 mV) on addition of Al^{3+} to its aqueous solution at pH 7.4. Therefore, indicating binding and subsequent aggregation of nanoparticles in presence of Al^{3+} (Wang et al., 2015). To further explore the binding between Al^{3+} and **HL-FeNPs**, we next recorded IR spectrum of the aggregate which reveals disappearance of the carboxyl OH stretching band. The carboxylate group of the aggregate displays a pair of bands at 1630 and 1405 cm^{-1} corresponding to the $\nu_{asym}(COO)$ and $\nu_{sym}(COO)$ vibrations, respectively. These vibrational frequencies suggest a bi-dented binding mode with characteristically large Δν (ca. 225 cm^{-1}) (Nickolov et al., 1995). In the light of hard-soft acid-base (HSAB) principle, carboxylate group is considered as hard base. Therefore, it will prefer to bind hard acids such as Cr^{3+}, Fe^{3+}, or Al^{3+}, used in this study. High ionic potential of Al^{3+} is most probably the driving force for the preferential chelation of Al^{3+} with **HL-FeNPs**. As illustrated schematically in Fig. 1d, Al^{3+} binds with three carboxylate groups to attain octahedral environment around the metal ion. This interactions between the nanosensor **HL-FeNPs** and Al^{3+} results in the aggregation of small sized nanoparticles to the clusters of reasonably large diameters. Therefore, we can state aggregation induced emission enhancement (AIEE) process is producing fluorescence

enhancement of **HL-FeNPs** in presence of Al^{3+} (Liu et al., 2013). The amorphous nature of the aggregate is also confirmed from the powder XRD pattern of the sample (Fig. S15).

*3.4 Removal of Al^{3+} present in aqueous solution using **HL-FeNPs***

Supermagnetism property of FeNPs was explored in this work to remove excess Al^{3+} from its aqueous solution using **HL-FeNPs**. For this purpose, different amounts of **HL-FeNPs** (100, 80, 60, 40, 20, and 0 mg) were dissolved in 8.5 ppm aqueous solution (50 mL) of Al^{3+}. The mixture was stirred at room temperature for 2 h and the dispersed substances was separated by the application of external magnet (inset, Fig. 5a). After Al^{3+} separation (as shown in Fig. 5a), the residual concentrations of Al^{3+} in water were measured by ICP-OES (Zhi et al., 2013). Removal ability of **HL-FeNPs** for other metal ions was also tested and Fig. 5b provided further evidence for specific affinity of the sensor towards Al^{3+}. Moreover, Fig. 5a demonstrates gradual decrease of Al^{3+} concentrations with increase in the quantity of **HL-FeNPs**. Upon addition of 100 mg **HL-FeNPs** to an 8.5 ppm aqueous solution of Al^{3+}, the concentration of Al^{3+} decreased to 0.15 ppm, after the magnetic separation of the analyte. This is well below than the US-EPA standard of dissolved Al^{3+} in drinking water (0.2 ppm) (Vallejos et al., 2015). For real world uses, it is obligatory to perform removal experiments with field samples. In this regards, seawater sample from Alang ship breaking yard was collected and tested for Al^{3+} enrichment after spiking with different metal ions. Results shown in Table S3, revealing undeniably non-interference of other metal ions in the effective Al^{3+} removal ability of **HL-FeNPs**.

3.5 In-situ bio-imaging and toxicity studies in live whole organism Artemia

Results from Table S1 and S2 undoubtedly reveals that nanoparticles based chemosensors are best fitted for bio-imaging applications. So far, only one report is available in

the literature on bio-imaging of Al^{3+}-specific probe in cell-lines and the biosensor was based on iron nanoparticles (Zhi et al., 2013). However, for real-time practical use of any chemosensor, *in-vivo* imaging with live organism is indispensable. For this purpose, we have studied a live whole brine shrimp *Artemia* which belongs to the subphylum crustacea. As the nanoprobe **HL-FeNPs** is made up of two bio-compatible components viz. the natural product 2,3-dihydroxybenzoylglycine and iron nanoparticles, we hypothesized that **HL-FeNPs** could sense Al^{3+} in higher group organisms. *Artemia* is a facile and cost-effective animal model suitable to explore for *in-vivo* bio-imaging experiments with live organism because of the features already mentioned in the literature (Nair et al., 2015; Giovanni, 2014; Turker and Usta, 2008).

Cultured brine shrimps after exposing to **HL-FeNPs** were examined under the microscope and the image displayed in Fig. 6a shows very weak fluorescence from the live organism. In *Artemia,* metal ion accumulations typically occurs in the gastrointestinal (GI) tract of the organism. The fluorescent image of live *Artemia* in presence of Al^{3+} showed blue colouration of the GI tract of *Artemia* (Fig. 6b) and therefore, demonstrating bio-magnification nature of the organism. Microscopic investigation with Al^{3+} failed to stain the GI-tract of *Artemia*. Observation through a light microscope revealed that **HL-FeNPs** is unable to visualize Al^{3+} colourimetrically in live animals (Fig. 6c). Overlay image, showed in Fig. 6d, confirmed that **HL-FeNPs** could indeed be used as a fluorescent biosensor for Al^{3+} in live organisms. Blue colouration of the GI tract of *Artemia* also confirmed the population of Al^{3+} in this region (Fig. 6b and 6d) of the live organism. To examine the reproducibility of the bio-imaging experiments with **HL-FeNPs** in live brine shrimps, same experiment was performed again and the result is shown in Fig. S16. Therefore, confirming the reproducibility of the nanobiosensor **HL-FeNPs** in visualizing Al^{3+} in live organism. To evaluate the practical bio-imaging potential of the above

method, Al^{3+} enrichment experiment was also performed using coastal seawater wherein Al^{3+} concentration was estimated to be <1 ppm. Results (Fig. S17) from bio-imaging experiments with spiked natural marine water unambiguously confer the real-world applicability of **HL-FeNPs** as a staining agent for Al^{3+} in live organisms.

Non-toxic nature of the nanobiosensor **HL-FeNPs** was also established from the mortality counting of *Artemia* cysts in presence of it. Results displayed in Table S4 demonstrates that siderophore derived nanobiosensor **HL-FeNPs** is a water soluble nontoxic biosensor which can detect and stain Al^{3+} fluorimetrically and *in-vivo* in live whole organism.

4. Conclusions

In this work, we have presented a novel nanobiosensor **HL-FeNPs** which is designed rationally based on the knowledge on binding affinities of microbial chelators for iron. Catechol type siderophore 2,3-dihydroxybenzoylglycine, upon anchoring on magnetic iron nanoparticles binds Al^{3+} very selectively in 100 % aqueous medium at pH 7.4 even in presence of other competing metal ions. The nanosensor **HL-FeNPs** could sense Al^{3+} rapidly and the limit of detection could reach 20 nM. Surface functionalization of iron nanoparticles with siderophore $\mathbf{H_3L}$ results in easy removal of excess Al^{3+} in aqueous solution by the use of external magnet. Furthermore, the use of water soluble and non-toxic siderophore to modify the surface of iron nanoparticles gives rise to the formation of a unique fluorogenic probe which can stain Al^{3+} in whole live organism and thus, establishing the biosensing property of the nanosensor. This is the first report on surface functionalization of iron nanoparticles by siderophore and its *in-vivo* bio-imaging application in live organism.

ACKNOWLEDGEMENTS

This work is supported by the Council of Scientific and Industrial Research (CSIR) under Pool Section (Pool No. 8821-A), New Delhi and CSIR Network Projects CSC 0105 and CSC 0134. We are indebted to AD&CIF of CSIR-CSMCRI for continued analytical support. The manuscript has been assigned CSMCRI 162/2016 registration number. SS thanks MANIT, Bhopal for financial support during her stay at CSIR-CSMCRI. IHR thanks DST, India for his JRF. We thank Dr. Parimal Paul and Dr. Bishwajit Ganguly for valuable discussions.

Appendix A. Supplementary materials

The Supplementary experimental details, figures (S1-S17) and tables (S1-S4) associated with this article can be found in the online version at

References

Benesi, H. A.; Hildebrand, J. H. 1949. J. Am. Chem. Soc. 71, 2703-2707.

Bugdahn, N.; Peuckert, F.; Albrecht, A. G.; Miethke, M.; Marahiel, M. A.; Oberthur, M. 2010. Angew. Chem., Int. Ed. 49, 10210-10213.

Cochrane, S. A.; Li, X.; He, S.; Yu, M.; Wu, M.; Vederas, J. C. 2015. J. Med. Chem. 58, 9779-9785.

Das, S.; Dutta, M.; Das, D. 2013. Anal. Methods 5, 6262-6285.

Doorneweerd, D. D.; Henne, W. A.; Reifenberger, R. G.; Low, P. S. 2010. Langmuir 26, 15424-15429.

Espinosa, A.; Corato, R. D.; Kolosnjaj-Tabi, J.; Flaud, P.; Pellegrino, T.; Wilhelm, C. 2016. ACS Nano 10, 2436-2446.

Farrell, D.; Cheng, Y.; McCallum, R. W.; Sachan, M.; Majetich, S. A. 2005. J. Phys. Chem. B 109, 13409-13419.

Garibaldi J. A.; Neilands, J. B. 1955. J. Am. Chem. Soc. 77, 2429-2430.

Giovanni, L. 2014. Marine Environ. Res. 101, 38-43.

Hasany, S. F.; Ahmed, I.; J, R.; Rehman, A. 2012. Nanosci. Nanotechnol. 2, 148-158.

Hider R. C.; Kong, X. 2010. Nat. Prod. Rep. 27, 637-657.

Hu, Y.; Wang, R.; Wang, S.; Ding, L.; Li, J.; Luo, Y.; Wang, X.; Shen, M.; Shi, X. 2016. Sci. Rep. 6, 28325.

Inomata, T.; Tanabashi, H.; Funahashi, Y.; Ozawa, T.; Masuda, H. 2013. Dalton Trans. 42, 16043-16048.

Ito, T.; Neilands, J. B. 1958. J. Am. Chem. Soc. *80*, 4645-4647.

Jin, J.; Yang, F.; Zhang, F.; Hu, W.; Sun, S.; Ma, J. 2012. Nanoscale 4, 733-736.

Johnstone T. C.; Nolan, E. M. 2015. Daltons Trans. 44, 6320-6339.

Jurkevitch, E.; Hadar, Y.; Chen, Y. 1986. J. Plant Nutr. 9, 535-545.

Lambert, S. G.; Taylor, J-. M.; Wegener, K. L.; Woodhouse, S. L.; Lincoln, S. F.; Ward. A. D. 2000. New J. Chem. 24, 541-546.

Li, W. P.; Liao, P. Y.; Su, C. H.; Yeh, C. S. 2014. J. Am. Chem. Soc. 136, 10062-10075.

Liu, H.; Hao, X.; Duan, C.; Yang, H.; Lv, Y.; Xu, H.; Wang, H.; Huang, F.; Xiao, D.; Tian, Z. 2013. Nanoscale 5, 9340-9347.

Margulies, D.; Melman, G.; Felder, C. E.; Arad-Yellin, R.; Shanzer, A. 2004. J. Am. Chem. Soc. 126, 15400-15401.

Miller, M. J.; Walz, A. J.; Zhu, H.; Wu, C.; Moraski, G.; Möllmann, U.; Tristani, E. M.; Crumbliss, A. L.; Ferdig, M. T.; Checkley, L.; Edwards, R. L.; Boshoff, H. I. 2011. J. Am. Chem. Soc. 133, 2076-2079.

Nair, R. R.; Raju, M.; Patel, N. P.; Raval, I. H.; Suresh, E.; Haldar, S.; Chatterjee, P. B. 2015. Analyst 140, 5464-5468.

Nel, A. E.; Mädler, L.; Velegol, D.; Xia, T.; Hoek, E. M. V.; Somasundaran, P.; Klaessig, F.; Castranova, V.; Thompson, M. 2009. Nat. Mater. 8, 543-557.

Nickolov, Zh.; Georgiev, G.; Stoilova, D.; Ivanov, I. 1995. J. Molec. Struct. 354, 119-125.

Noël, S.; Guillon, L.; Schalk, I. J.; Mislin, G. L. A. 2011. Org. Lett. 13, 844-847.

Pal, S.; Alocilj, E. C. 2010. Biosens. Bioelectron. 26, 1624–1630.

Pu, K.; Shuhendler, A. J.; Jokerst, J. V.; Mei, J.; Gambhir, S. S.; Bao, Z.; Rao, J. 2014. Nat. Nanotechnol. 9, 233-239.

Raju, M.; Nair, R. R.; Raval, I. H.; Haldar, S.; Chatterjee, P. B. 2015. Analyst 140, 7799-7809.

Raju, M.; Patel, T. J.; Nair, R. R. Chatterjee, P. B. 2016. New J. Chem. 40, 1930-1934.

Raymond, K. N.; Dertz, E. A.; Kim, S. S. 2003. Proc. Natl. Acad. Sci. U. S. A. 100, 3584-3588.

Sandy, M.; Butler, A. 2009. Chem. Rev. 109, 4580-4595.

Sasikala, A. R. K.; Thomas, R. G.; Unnithan, A. R.; Saravanakumar, B.; Jeong, Y. Y.; Park, C. H.; Kim, C. S. 2016. Sci. Rep. 6, 20543.

Sharma, R. K.; Kumar, H.; Kumar, A. 2015. RSC Adv. 5, 43371-43380.

Shubayev, V. I.; Pisanic II, T. R.; Jin, S. 2009. Adv. Drug Deliv. Rev. 61, 467-477.

Soulere, L.; Viode, C.; Perie, J.; Hoffmann, P. 2002. Chem. Pharm. Bull. 50, 578-582.

Sun, S.; Zeng, H.; Robinson, D. B.; Raoux, S.; Rice, P. M.; Wang, S. X.; Li, G. 2004. J. Am. Chem. Soc. 126, 273-279.

Tang, C.; Russell, P. J.; Wilks, R. M.; Rasko, J. E. J.; Khatri, A. 2010. Stem Cells 28, 1686-1702.

Turker A. U.; Usta, C. 2008. Nat. Prod. Res. 22, 136-146.

Vallejos, S.; Munoz, A.; Ibeas, S.; Serna, F.; Garcia, F. C.; Garcia, J. M. 2015. ACS Appl. Mater. Interfaces 7, 921-928.

Wang, B.; Hai, J.; Liu, Z.; Wang, Q.; Yang, Z.; Sun, S. 2010. Angew. Chem. Int. Ed. 49, 4576-4579.

Wang, B.; Hai, J.; Wang, Q.; Li, T.; Yang, Z. 2011. Angew. Chem. Int. Ed. 50, 3063–3066.

Wang, B. D.; Xu, C. J.; Xie, J.; Yang, Z. Y.; Sun, S. H. 2008. J. Am. Chem. Soc. 130, 14436-14437.

Wang, T.; Yang, W.; Song, T.; Li, C.; Jhang, L.; Wang, H.; Chai, L. 2015. RSC Adv. 5, 50011-50018.

Wang, X.; Stolwijk, J. A.; Lang, T.; Sperber, M.; Meier, R. J.; Wegener, J.; Wolfbeis, O. S. 2012. J. Am. Chem. Soc. 134, 17011-17014.

Wu, S. M.; Zhang, Z. L.; Wang, X. D.; Zhang, M. X.; Peng, J.; Xie, Z. X.; Pang, D. W. 2009. J. Phys. Chem. C 113, 9169-9174.

Xian, Z.; Panyue, Z.; Zhen, W.; Ling, Z.; Guangming, Z.; Chunjiao, Z. 2013. Colloids Surf. A 435, 85-90.

Xu, Z.; Shen, C.; Hou, Y.; Gao, H.; Sun, S. 2009. Chem. Mater. 21, 1778-1779.

Zhang, H.; Zeng, X.; Chen, D.; Guo, Y.; Jiang, W.; Xu, L.; Fu, F. 2015. RSC Adv. 5, 45847-45852.

Yang, Z.; Shaofei, Y.; Qian, L.; Dandan, Y.; Yun, W.; Li, G.; Juan, H.; Haifeng, S. 2017. Sci. Rep. 7, 41741.

Zheng, T.; Bullock, J. L.; Nolan, E. M. 2012. J. Am. Chem. Soc. 134, 18388-18400.

Zheng, T.; Nolan, E. M. 2014. J. Am. Chem. Soc. 136, 9677-9691.

Zheng, T.; Nolan, E. M. 2012. Metallomics 4, 866-880.

Zhi, L.; Liu, J.; Wang, Y.; Zhang, W.; Wang, B.; Xu, Z.; Yang, Z.; Huo, X.; Li, G. 2013. Nanoscale 5, 1552-1556.

Zhou, Y.; Yuan, S.; Liu, Q.; Yan, D.; Wang, Y.; Gao, L.; Han, J.; Shi, H. 2017. Sci. Rep. **7**, 41741.

Fig. 1. Pictorial representations of (a) siderophore **H_3L** (b) oleylamine coated bare FeNP and (c) siderophore functionalized iron nanoparticle (i.e. **HL-FeNP**). (d) Schematic presentation of the mechanism of Al^{3+} detection by **HL-FeNPs**.

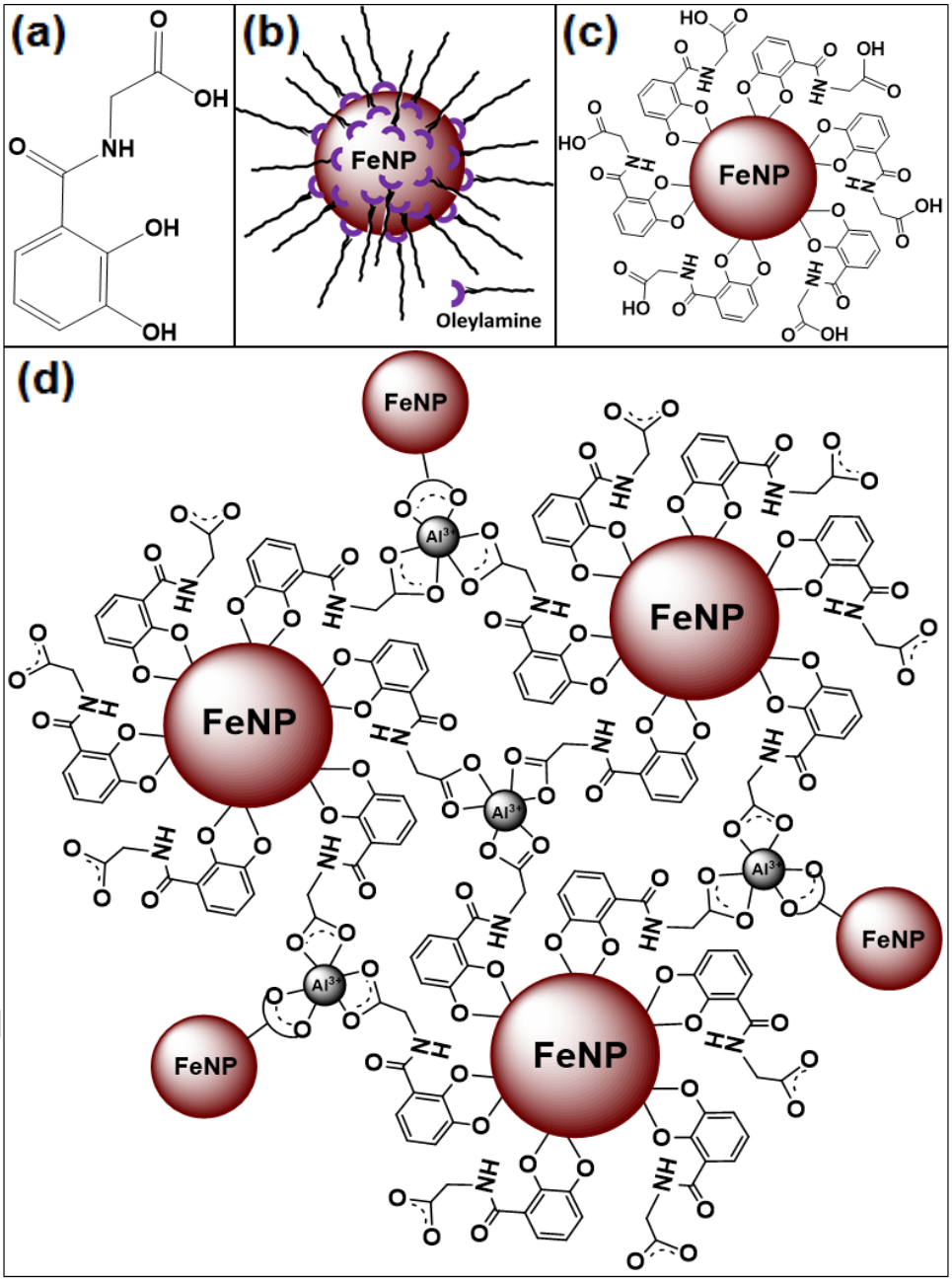

Fig. 2. Typical TEM image (a) and FTIR-ATR spectrum (b) of **HL-FeNPs**. Particle sizes distribution of **HL-FeNPs** from DLS experiment (c) and powder XRD pattern of **HL-FeNPs**.

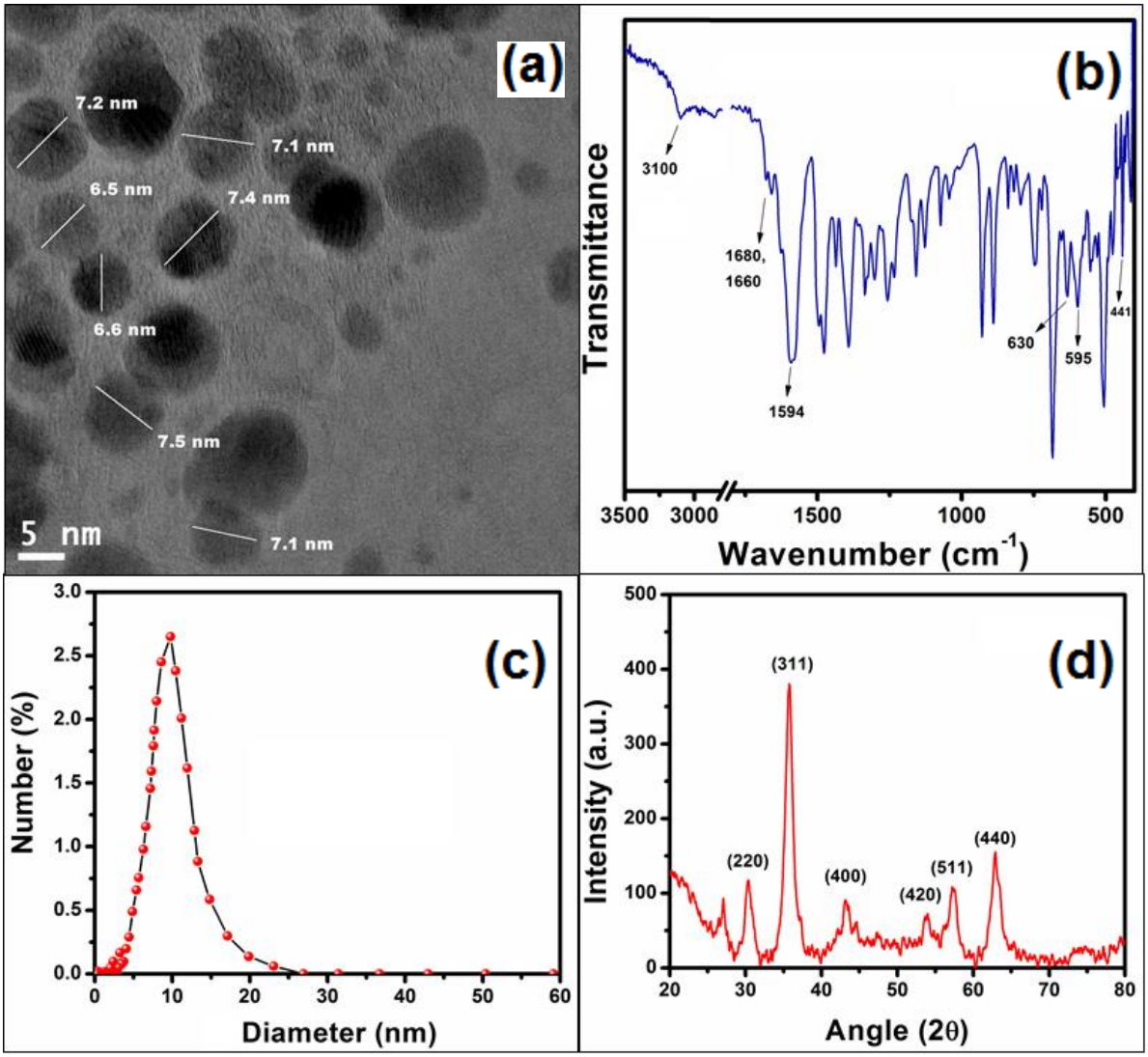

Fig. 3. Fluorescence spectra of **HL-FeNPs** alone and in presence of different metal ions

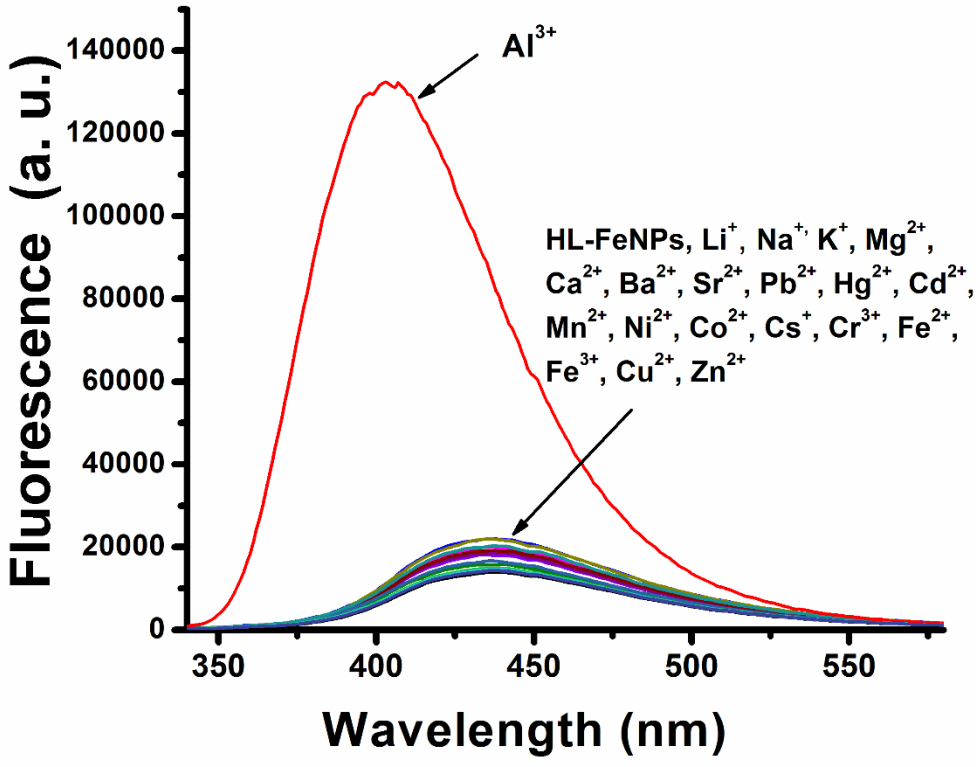

Fig. 4. Bar diagrams showing fluorescence peak intensities of a mixture of **HL-FeNPs** and Al^{3+} in the presence of each of other metal ions (4 equivalents) in HEPES aqueous buffer solution (pH 7.4). Each column represents the average of three experiments and error bars are the relative standard deviations.

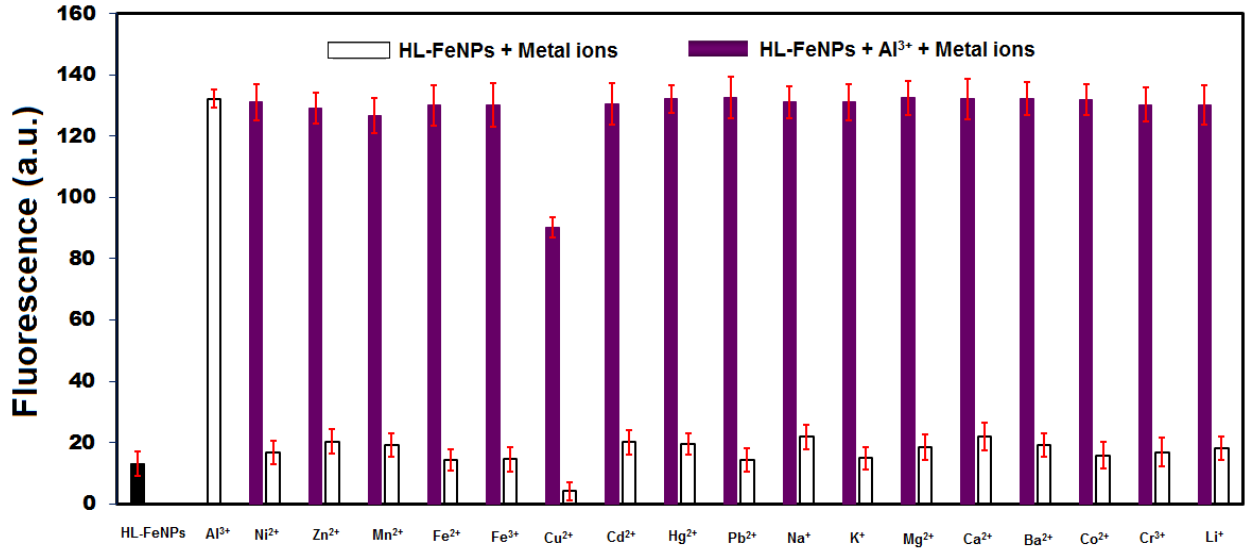

Fig. 5. ICP plots showing residual concentrations of Al^{3+} after its removal from Al^{3+} enriched aqueous solutions using different amounts of **HL-FeNPs**. Each column represents the average of three data and error bars are the relative standard deviations. Inset: the removal of excess Al^{3+} from its aqueous solution with the use of an external magnet and **HL-FeNPs**.

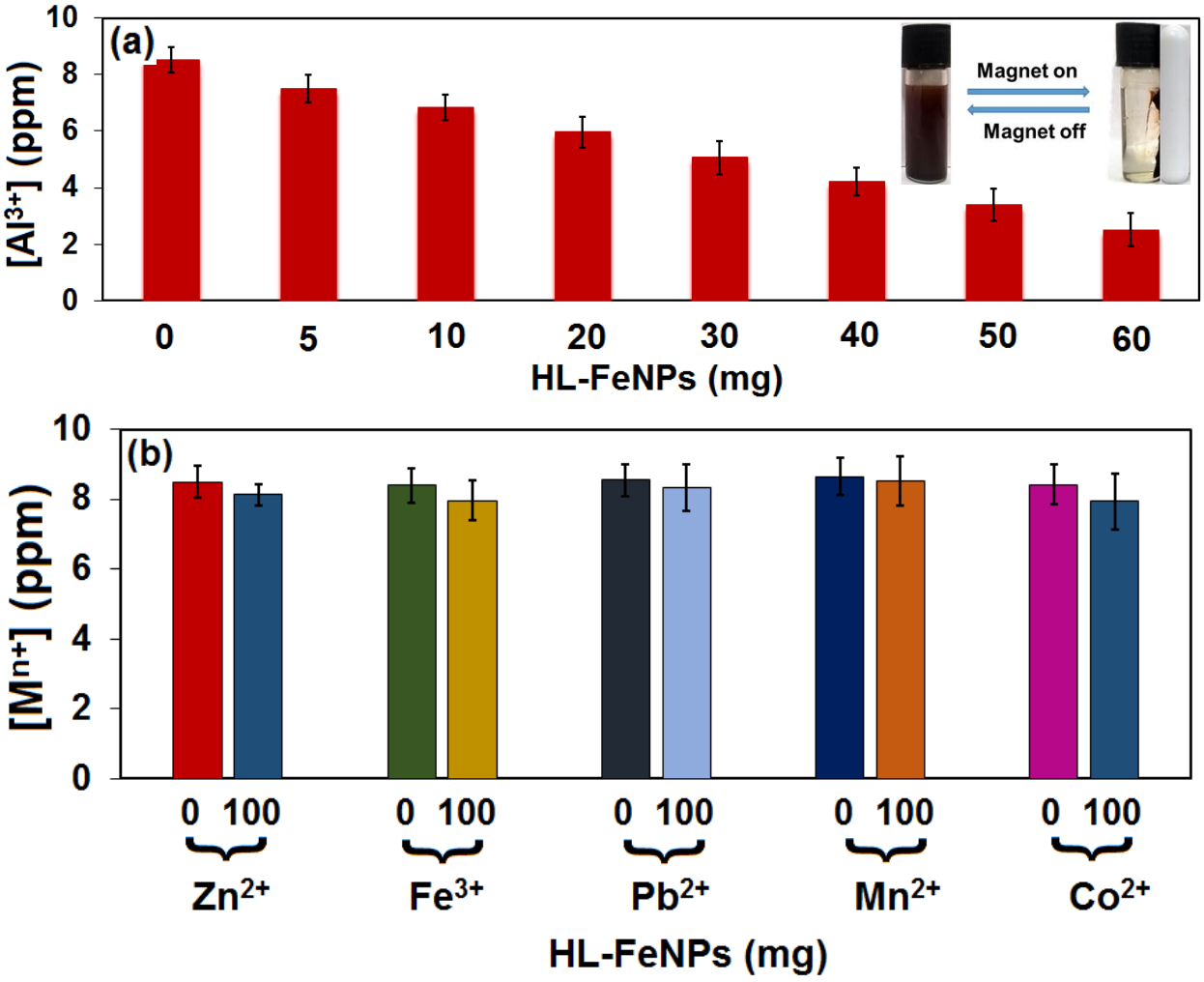

Fig. 6. Fluorescent images of live whole *Artemia* exposed to (a) **HL-FeNPs** alone and (b) 10 μM Al^{3+} followed by the addition of **HL-FeNPs**. (c) Bright field microscopic images of live *Artemia* exposed to 10 μM Al^{3+} followed by the addition of **HL-FeNPs**. (d) Overlap image of panel c and b. Arrows indicate the position of GI tract of *Artemia*.

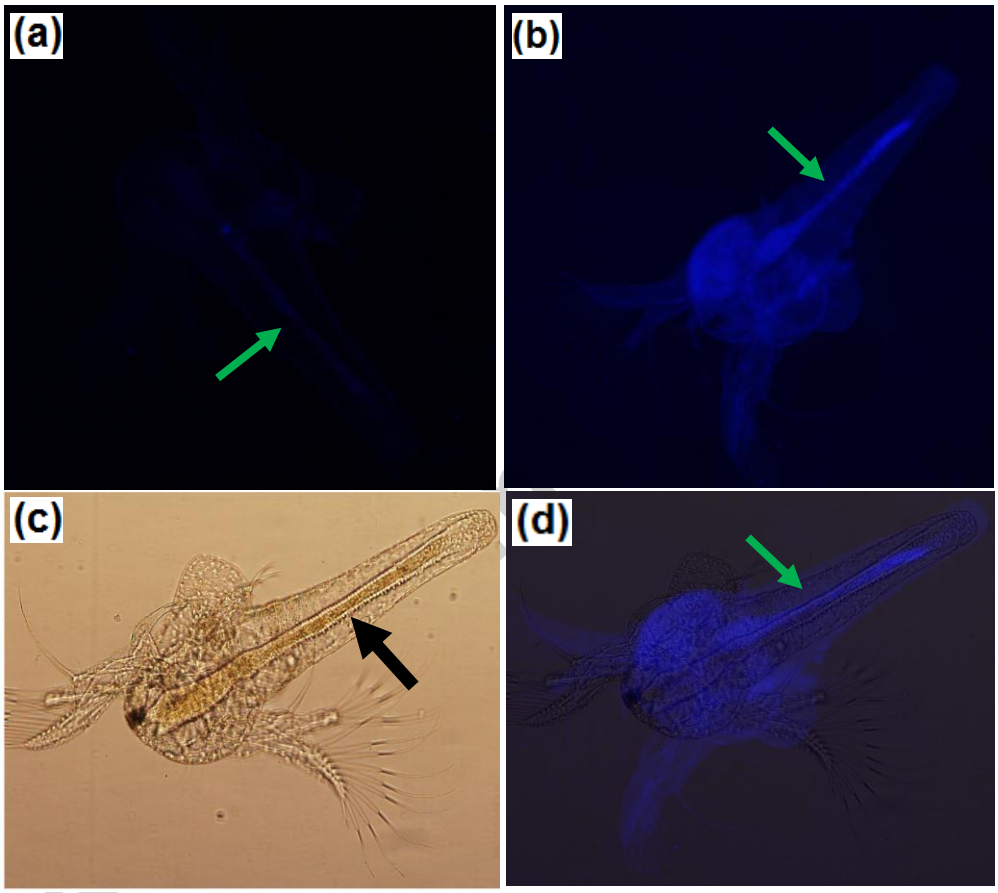

Highlights

- Rational fabrication of the surface of iron nanoparticles by a microbial chelator which inherently possess high affinity for iron.

- Synthesis and characterization of siderophore functionalized iron nanoparticles **HL-FeNP** for sensing Al^{3+} in 100 % water.
- Live organism *in-vivo* bio-imaging of Al^{3+} by the nanobiosensor **HL-FeNP**.
- Magnetic nanobiosensor **HL-FeNP** can be used to remove excess Al^{3+} from aqueous sample collected from natural sources.